

Nanometer-scale material contrast imaging with a near-field microwave microscope

Atif Imtiaz^{a)} and Steven M. Anlage

Center for Superconductivity Research, Department of Physics, University of Maryland, College Park, Maryland 20742-4111

John D. Barry and John Melngailis

Institute for Research in Electronics and Applied Physics, University of Maryland, College Park, Maryland 20742-3511

(Received 3 January 2007; accepted 26 February 2007; published online 3 April 2007)

The authors report topography-free material contrast imaging on a nanofabricated boron-doped silicon sample measured with a near-field scanning microwave microscope over a broad frequency range. The boron doping was performed using the focus ion beam technique on a silicon wafer with nominal resistivity of 61 Ω cm. A topography-free doped region varies in sheet resistance from 1000 Ω/\square to about 400 k Ω/\square within a lateral distance of 4 μm . The qualitative spatial resolution in sheet resistance imaging contrast is no worse than 100 nm as estimated from the frequency shift signal. © 2007 American Institute of Physics. [DOI: 10.1063/1.2719164]

As complementary metal-oxide-semiconductor technology reaches the sub-45-nm node, and operating frequencies of integrated circuits reach into the microwave regime, there is a strong need to quantitatively measure local material properties at microwave frequencies with nanometer spatial resolution.^{1,2} For example, there is a need to develop metrological tools to characterize ultrashallow-doped films for submicron semiconductor devices,³ which requires local measurement of material properties such as sheet resistance (R_x). Similarly, metrological tools are required to understand the basic physics of carbon nanotubes and nanowires before they become useful for electronics.¹ To achieve such goals, near-field scanning microwave microscopes (NSMMs) have been developed as quantitative metrology tools,^{4,5} and with such microscopes, the local R_x has been measured with spatial resolution on the micrometer length scale.^{6–8} However, sample topography affects the measured NSMM signals⁹ and it is quite challenging to separate the topographic effects from material properties.⁷ Such challenges raise questions regarding the ability of NSMM to be a useful metrology tool for nanoscience and nanotechnology. In order to demonstrate the NSMM as a useful metrology tool at such length scales, we designed a topography-free sample with varying R_x on the nanometer length scale. This sample, prepared using focused ion beam (FIB) implantation¹⁰ (described in detail elsewhere^{11,12}), has been measured with a high-resolution NSMM which utilizes scanning tunneling microscopy (STM) for distance-following¹³ and is capable of measuring R_x variations of thin films.⁷

The sample is a $10 \times 10 \mu\text{m}^2$ patch with a sheet resistance gradient ranging from $R_x=30$ to $5.5 \times 10^5 \Omega/\square$ over a lateral length scale of 10 μm (Fig. 1). However, the topography-free region has values in the range $R_x=10^3$ – $4 \times 10^5 \Omega/\square$, as will be discussed shortly. The STM topography image of the variable- R_x region of the sample is shown in Fig. 1(a). Because the doping concentration is constant in the vertical direction, we can take the average lateral line cuts of STM topography [the open squares in Fig. 1(b), right

vertical axis]. The calculated R_x profile of the sample as a function of position is also shown in Fig. 1(b) (the dashed line, left vertical axis). This R_x profile is calculated using the FIB beam parameters¹⁰ and the knowledge of the implanted boron depth and profile.^{11,12} The region of high boron concentration (and low R_x) is on the left side of the sample. This part of the sample is damaged [labeled so in Fig. 1(b)] because the beam dwell time was very long on this region to dope to a high concentration. As a result there is roughly 10 nm of topography present in the high boron concentration region. The extreme right hand side of the doped area close to the undoped silicon also shows some topography of about 5 nm. In between, there is a lateral region of 4 μm which on average has zero (± 1 nm) topography, labeled as “topography-free” region in Fig. 1(b). This is a good region for maintaining a constant height of the probe above the sample, while the NSMM contrast here is expected to be due to the changes in R_x alone.

While maintaining the NSMM probe at a constant height of 1 nm above the sample,¹⁴ the quality factor (Q) and fre-

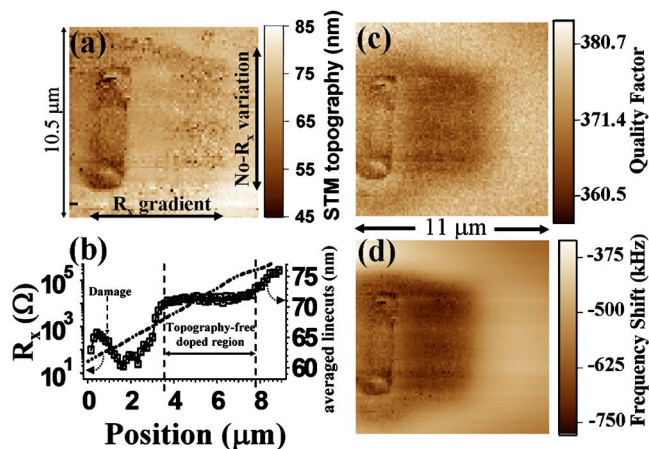


FIG. 1. (Color online) (a) STM topography and (b) the average of horizontal line cuts taken from the topography image, along with the calculated R_x profile. (c) Quality factor and (d) frequency shift images. The microscope frequency is 7.472 GHz, and the tunnel current set point for these simultaneous images is 0.5 nA with bias of 1 V.

^{a)}Electronic mail: atif@boulder.nist.gov

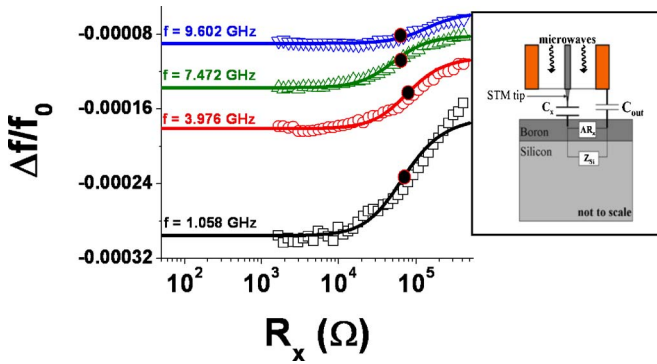


FIG. 2. (Color online) Symbols show the averaged $\Delta f/f_0$ line cuts through Fig. 1(d) for four different frequencies. Also shown are $\Delta f/f_0$ fits to the data, where f_0 is the resonant frequency with no sample present. The inset shows the lumped-element model used to fit the data. The fit parameters are given in Table I. The dots on the curve signify points where $\omega C_x(AR_x)=1$.

quency shift (Δf) images were acquired, as shown in Figs. 1(c) and 1(d) where the frequency of the experiment is 7.472 GHz. The doped region clearly shows Q and Δf contrast in the topography-free region. The NSMM responds to the variable- R_x region of the sample through both reactive and resistive interactions with the sample. The NSMM also responds to the damaged (strong topography) area. Since the sample has no R_x variation in the vertical direction, one can take lateral line segments at a fixed vertical position from the topography-free area, and average them together to form the line cuts (shown in Fig. 2 for Δf and in Fig. 3 for Q). The data over the region of damage (as seen on the left side of the images) and the data with topography close to bare silicon on the right are not shown in these averages. Similar images and analysis were also obtained at microwave frequencies of 1.058, 3.976, and 9.602 GHz, with all experiments performed at room temperature.

A lumped-element model⁴ of the microscope/sample interaction used to understand the data is shown schematically in the inset of Fig. 2. The sample in this case is a thin doped layer with circuit impedance AR_x , on top of bulk silicon, with

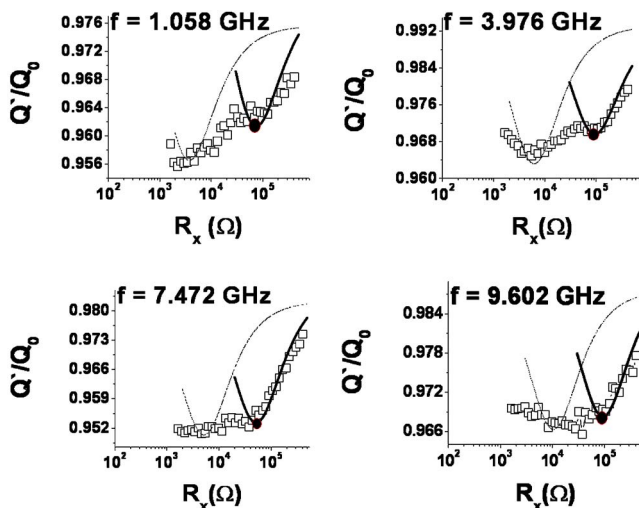


FIG. 3. Symbols show the averaged Q'/Q_0 line cuts through Fig. 1(c) for four different frequencies. Also shown are the Q'/Q_0 fits to the data, where Q_0 is the quality factor of the resonator with no sample present. The fit parameters (see Table I) for the low- R_x data (dashed lines) differ from the high- R_x data (solid lines). The dots on the curve signify points where $\omega C_x(AR_x)=1$.

impedance Z_{Si} . R_x is the sheet resistance of the doped layer and A is a geometrical coefficient relating the circuit impedance to the field impedance,⁴ which arises due to the geometry of the probe and the presence of different boundary conditions^{15,16} in the sample. The substrate impedance Z_{Si} includes the resistivity ρ_{sub} of the bulk silicon ($\rho_{sub}=61 \Omega \text{ cm}$) and the (assumed real) dielectric constant ($\epsilon_{Si}=11.9$). The capacitance between the (STM tip) inner conductor of the transmission line resonator and the sample is labeled as C_x , and the capacitance between the sample and outer conductor is labeled as C_{out} [$C_{out} (\sim \text{pF}) \gg C_x (\sim \text{fF})$].

The expressions⁴ to calculate the quality factor and frequency shift from the near-field model include the following parameters. The transmission line resonator (with characteristic impedance $Z_0=50 \Omega$, attenuation α , mode number n , and length L_{res}) is terminated by the STM tip (electrical tip), with a characteristic size (called D_t) and the sample. The tip and the sample together have impedance Z_{tE} which is the sum of the resistive (R_{tE}) and the reactive (X_{tE}) impedances. Assuming that $|Z_{tE}| \gg Z_0$, the complex reflection coefficient² is calculated (for the geometry shown in the inset of Fig. 2) for the resonant condition of the transmission line resonator. This yields predictions for the quality factor Q' and relative frequency shift $\Delta f/f_0$ for the resonator as shown in Ref. 4. The effective dielectric constant of the resonator is $\epsilon_{eff}=2.5$, $L_{res}=1.06 \text{ m}$, and attenuation α is frequency dependent (0.0673 Np/m at 1.058 GHz to 0.209 Np/m at 9.602 GHz).

The R_x contrast in the $\Delta f/f_0$ signal saturates below an R_x of about $10 \text{ k}\Omega/\square$ and above about $400 \text{ k}\Omega/\square$ for this probe geometry and frequency range, as seen in Fig. 2. For the R_x values in between, the signal shows the largest contrast range. We expect the sensitivity of microscope frequency shift to sheet resistance to be maximized near the condition that the magnitude of the capacitive reactance is equal to the resistive impedance of the sample presented to the probe tip.¹³ This is true for all frequencies, as we note that $\omega C_x(AR_x) \cong 1$ roughly in the middle of the $\Delta f/f_0$ contrast range (dots in Fig. 2). For example, for the frequency of 1.058 GHz, this point is near $R_x=75 \text{ 000 } \Omega/\square$ and $\omega C_x(AR_x)=1.2$. The Q'/Q_0 versus sheet resistance data (Fig. 3, where Q_0 is the quality factor with no sample present) also show a local minimum where the magnitude of the capacitive reactance is equal to the resistive impedance (shown as black dots) of the sample presented to the probe tip.^{7,13}

To fit the data in Figs. 2 and 3, the probe characteristic dimension D_t was fixed to $15 \mu\text{m}$ [which is twice the typical R_0 value when the probe is regarded as a sphere of radius R_0 (Ref. 14)]. The other fitting parameters are the tip-sample capacitance C_x and the geometrical factor A . In Figs. 2 and 3 we show the fit to the $\Delta f/f_0$ and Q'/Q_0 data (solid lines), respectively, at different frequencies, with the fit parameters shown in Table I. The fits to $\Delta f/f_0$ vs R_x for all frequencies are excellent, while the same fits also describe the high- R_x Q'/Q_0 data quite well. The C_x fit value systematically decreases as the frequency increases because the tip-sample capacitance C_x can be regarded as a series combination of two capacitors: one from the geometry of the tip and the sample ($C_{geometry}$) and the second is the material dependent capacitor ($C_{material}$).¹⁷ The skin depth of the silicon substrate is also decreasing as the frequency increases, and as a result the value of ($C_{material}$) is effectively increasing. Hence, at higher frequencies, ($C_{geometry}$) is becoming the more domi-

TABLE I. Fit parameter (C_x, A) values for the fits shown as solid lines in Figs. 2 and 3 at the corresponding frequencies for fixed probe characteristic dimension D . The A parameter values in the brackets fit the low- R_x quality factor data minima and create the fits shown as dashed lines in Fig. 3.

f (GHz)	D_t (μm)	C_x (fF)	A
1.058	15	16.5	0.15 (3)
3.976	15	10.3	0.05 (0.65)
7.472	15	7.7	0.05 (0.50)
9.602	15	5.0	0.047 (0.27)

nant capacitor approaching the value (≈ 1 fF) we expect for tip-sample capacitance¹³ calculated from a conducting sphere above an infinite conducting plane model.

Besides the tip-sample capacitance C_x , the other fitting parameter is A , which links the material properties of the sample to Z_{TE} , and is dependent on the geometry of the tip⁴ and the sample.^{15,16} For an ideal coaxial Corbino-geometry contact (with $r_{\text{out}}=840 \mu\text{m}$ and $r_{\text{in}}=255 \mu\text{m}$), we expect the value of A to be 0.19.¹⁸ However, A can vary if the geometry deviates from the right-cylindrical Corbino structure, which is the case in our system due to a conical tip (with embedded sphere at the end¹⁴) and the geometrical features on the sample (with and without topography). The nontopographic features on the sample include the $10 \times 10 \mu\text{m}^2$ boron-doped patches and the finite thickness of the silicon wafer (smaller than both the wavelength and the skin depth for the measured frequency range). The geometrical features with topography (in the low- R_x region) are about $4 \times 10 \mu\text{m}^2$ in size. The presence of topography in this region increases the dissipated power locally,¹⁶ affecting primarily the quality factor, as seen in Fig. 3 for Q'/Q_0 in the low- R_x region (the value of A in parentheses in Table I fits the minimum in this region). As the frequency of measurement increases, the value of A decreases due to the decreasing skin depth and associated changes in field configuration.

To conclude, the boron-doped silicon sample has a $4 \times 10 \mu\text{m}^2$ region of topography-free variable sheet resistance. This region shows a continuous variation in R_x from values of $1000 \Omega/\square$ – $400 \text{k}\Omega/\square$. As seen in Fig. 2, the frequency shift signal shows a clear contrast in this region. Looking at the data in the region where the magnitude of the capacitive reactance is equal to the resistive impedance of the sample presented to the probe tip [$\omega C_x (AR_x) \cong 1$], two

data points that are 100 nm apart on the sample show a clear and distinct contrast in $\Delta f/f_0$. This suggests that the quantitative spatial resolution in R_x is no worse than 100 nm for the NSMM employed here (consistent with Ref. 13). By designing probes with larger values of the geometry factor A , one can increase sensitivity to lower- R_x films and materials while maintaining high spatial resolution.

The authors thank Andrew Schwartz and Vladimir Talanov of Neocera/Solid State Measurements, Inc. for insightful discussions. This work has been supported by NSF GOALI (DMR-0201261) and NSF/ECS-0322844.

¹Semiconductor Industry Association, *International Technology Roadmap for Semiconductors*, updated 2004 (<http://www.itrs.net/>).

²B. T. Rosner and D. W. van der Weide, *Rev. Sci. Instrum.* **73**, 2505 (2002).

³B. El-Kareh, *J. Vac. Sci. Technol. B* **12**, 172 (1994).

⁴S. M. Anlage, V. V. Talanov, and A. R. Schwartz, in *Scanning Probe Microscopy: Electrical and Electromechanical Phenomena at the Nanoscale*, edited by S. Kalinin and A. Gruverman (Springer, New York, 2007), Vol. 1, pp. 215–253.

⁵V. V. Talanov, A. Scherz, R. L. Moreland, and A. Schwartz, *Appl. Phys. Lett.* **88**, 134106 (2006).

⁶D. E. Steinhauer, C. P. Vlahacos, S. K. Dutta, F. C. Wellstood, and S. M. Anlage, *Appl. Phys. Lett.* **71**, 1736 (1997).

⁷D. E. Steinhauer, C. P. Vlahacos, S. K. Dutta, B. J. Feenstra, F. C. Wellstood, and S. M. Anlage, *Appl. Phys. Lett.* **72**, 861 (1998).

⁸S. Hyun, J. H. Cho, A. Kim, J. Kim, T. Kim, and K. Char, *Appl. Phys. Lett.* **80**, 1574 (2002).

⁹B. Hecht, H. Bielefeldt, Y. Inouye, D. W. Pohl, and L. Novotny, *J. Appl. Phys.* **81**, 2492 (1997).

¹⁰J. Melngailis, *J. Vac. Sci. Technol. B* **5**, 469 (1987).

¹¹A. Imtiaz, M. Pollak, S. M. Anlage, J. D. Barry, and J. Melngailis, *J. Appl. Phys.* **97**, 044302 (2005).

¹²Nine such patches were created in the form of a 3×3 array with separation of $10 \mu\text{m}$ from each other in the lateral and vertical directions on n -type silicon. Four out of nine features showed consistent, reproducible results like those discussed here, while other features showed large topography due to surface contamination. With an FIB beam energy of 30 keV the depth of implant has a mean value of 100 nm.

¹³A. Imtiaz and S. M. Anlage, *Ultramicroscopy* **94**, 209 (2003).

¹⁴A. Imtiaz and S. M. Anlage, *J. Appl. Phys.* **100**, 044304 (2006).

¹⁵H. Bhimnathwala and J. M. Borrego, *J. Vac. Sci. Technol. B* **12**, 395 (1994).

¹⁶C. L. Holloway and E. F. Kuester, *IEEE Trans. Microwave Theory Tech.* **48**, 1601 (2000).

¹⁷J.-P. Bourgoin, M. B. Johnson, and B. Michel, *Appl. Phys. Lett.* **65**, 2045 (1994).

¹⁸J. C. Booth, D. H. Wu, and S. M. Anlage, *Rev. Sci. Instrum.* **65**, 2082 (1994).